Chemical Science

Accepted Manuscript

This article can be cited before page numbers have been issued, to do this please use: X. Lv, M. Sun, L. Xu, R. Wang, H. Zhou, Y. Pan, S. Zhang, Q. sun, S. Xue and W. Yang, *Chem. Sci.*, 2020, DOI: 10.1039/D0SC01341B.

ROYAL SOCIETY OF CHEMISTRY

rsc.li/chemical-science

View Article Online
DOI: 10.1039/D0SC01341B

ARTICLE

Highly Efficient Non-doped Blue Fluorescent OLEDs with Low Efficiency Roll-off Based on Hybridized Local and Charge Transfer Excited State Emitters†

Received 00th January 20xx,
Accepted 00th January 20xx

DOI: 10.1039/x0xx00000x

Xianhao Lv,‡[a] Mizhen Sun,‡[a] Lei Xu,[a] Runzhe Wang,[a] Huayi Zhou,[a] Yuyu Pan,[b] Shitong Zhang,[c] Qikun Sun, [a] Shanfeng Xue*[a] and Wenjun Yang [a]

Designing a donor-acceptor (D-A) molecule with a hybridized local and charge transfer (HLCT) excited state is a very effective strategy for producing an oganic light-emitting diode (OLED) with a high exciton utilization efficiency and external quantum efficiency. Herein, a novel twisting D-π-A fluorescent molecule (triphenylamine-anthracene-phenanthroimodazole; TPAAnPI) is designed and synthesized. The excited state properties of the TPAAnPI investigated through photophysical experiments and density functional theory (DFT) analysis reveal that its fluorescence is due to the HLCT excited state. The optimized non-doped blue OLED using TPAAnPI as light-emitting layer exhibits a novel blue emission with a electroluminescence (EL) peak at 470 nm, corresponding to the Commission International de L'Eclairage (CIE) coordinates of (0.15, 0.22). A fabricated device termed Device II exhibits a maximum current efficiency of 18.09 cd A^{-1}, power efficiency of 12.35 lm W^{-1}, luminescence of ≈29900 cd cm^{-2}, and external quantum efficiency (EQE) of 11.47%, corresponding to a high exciton utilization efficiency of 91%. Its EQE remains as high as 9.70% at a luminescence of 1000 cd m^{-2} with low efficiency roll-off of 15%. These results are among the best for HLCT blue-emitting materials involved in non-doped blue fluorescent OLEDs. The performance of Device II highlights a great industrial application potential for the TPAAnPI molecule.

Introduction

Organic light-emitting diodes (OLEDs) exhibit impressive advantages in full colour flat-panel displays and solid-state luminescence due to their high luminous efficiency and brightness, wide field-of-view, flexibility, and low cost.[1-4] Although red and green emitting materials exhibit satisfactory performances, the acquisition of high-performance blue-emitting materials involving high efficiency and novel colour purity remains a major challenge. This is due to the intrinsic wide bandgaps of blue emitters, which generates a high charge-injection barrier and unbalanced charge-injection and transportation.[5] Internal quantum efficiency (η_{int}) up to 100% can be obtained for some blue phosphorescent OLEDs (phOLEDs) based on Ir, Pt, and Os complexes. However, some distinct disadvantages such as introducing valuable metals, low photoluminescence quantum efficiency, and deficiency of excellent blue phosphorescent materials still exist. Also, phosphorescent materials necessitate dispersion into proper host materials with large band gaps to reduce the quenching effect of long-lived triplet excitons.[6] Therefore, novel metal-free blue fluorescent materials suitable for producing low cost non-doped OLEDs with high efficiency are needed. Thermally-activated delayed fluorescence (TADF)[7] and hybridized local and charge transfer (HLCT)[8] are two recently reported mechanisms that can yield 100% exciton utilization efficiency (EUE) in blue fluorescent OLEDs. In TADF emitters, the highest occupied molecular orbital (HOMO) and lowest unoccupied molecular orbital (LUMO) separation is demonstrated by proper selection and linkage of donor (D) and acceptor (A) moieties to form a D-A molecular structure, with blue-emissive OLED EQE capable of attaining 30%.[9] However, like phosphorescent OLEDs, their EQE are commonly affected by severe roll-off at a high current density due to cumulated triplet excited states. Therefore, TADF materials require doping into host materials with high triplet energy, which increases their fabrication cost.[10]

Similar to the TADF mechanism, the CT excited state component in HLCT excited state facilitates the efficient reverse intersystem crossing (RISC) process by the small ΔE_{ST}, accounting for the high EUE. However, unlike TADF emitters, the HLCT-type emitters display short excited lifetimes, which are favourable for fabricating cheap high-efficiency non-doped OLEDs. Especially, in some blue-emissive weekly-coupled HLCT materials, the final emissive excited state is a nearly pure locally excited (LE) state rather than a CT excited state. This is beneficial for the blue-shift

[a] Key Laboratory of Rubber-Plastics of the Ministry of Education/Shandong Province (QUST), School of Polymer Science & Engineering, Qingdao University of Science &Technology, 53-Zhengzhou Road, Qingdao 266042, P. R. China. E-mail: sfxue@qust.edu.cn
[b] School of Petrochemical Engineering, Shenyang University of Technology, 30 Guanghua Street, Liaoyang, 111003, P. R. China
[c] State Key Laboratory of Supramolecular Structure and Materials, Jilin University, Changchun, 130012, P. R. China.

† Electronic Supplementary Information (ESI) available: Details of synthesis and characterization, general methods, detailed PL and EL performance and detailed TDDFT calculations, DSC curves, TGA curves, CV curves and the transient EL decay curves of device.

‡ Xianhao Lv and Mizhen Sun contributed equally to this work.

emission wavelength due to a shortened lifetime and satisfactory efficiency.[11]

In this study, we designed and synthesized a novel blue HLCT molecule, the TPAAnPI. In this molecule, triphenylamine (TPA) is a moderate electron-donating moiety with propeller conformation, while phenanthroimidazole (PI) represents a highly efficient violet-blue chromophore with moderate electron-accepting ability. Anthracene acts as a conjugated core linking TPA and PI. Hence, the twisting D-π-A molecular conformation and the moderate electron donating and accepting ability can facilitate the partial separation of HOMO and LUMO, thereby improving the CT component in the molecule. The presence of the anthracene moiety increases the conjugation length and improves the LE component. Concurrently, the 9,10-substituted anthracene enhances the twisting, which efficiently prevents the aggregation-caused quenching effect.

The photophysical experiments and density functional theory (DFT) calculation manifest that the emissive state of TPAAnPI is a HLCT state. The TPAAnPI exhibits a novel blue emission with a PL peak at 470 nm both in THF and solid film state, with photo-luminescent quantum yield (PLQY) of TPAAnPI of 0.71 and 0.42, respectively. We fabricated the TPAAnPI non-doped Device I, which shows a novel blue emission with the electroluminescence (EL) emission peak at 470 nm, corresponding to the Commission International de L'Eclairage (CIE) coordinates of (0.15,0.22). The maximum external quantum efficiency (EQE) is 8.00% at a luminance of 705 cd m^{-2}. Although the efficiency roll-off is only of 0.75% at the luminance of 1000 cd m^{-2}, the EQE remains unsatisfactory for industrial application. Further, the optimized non-doped Device II exhibited a maximum CE of 18.09 cd A^{-1}, PE of 12.35 lm W^{-1}, luminescence of ≈ 29900 cd cm^{-2}, and EQE of 11.47%, corresponding to a high EUE of 91%. More importantly, the EQE remains as high as 9.70% at a luminescence of 1000 cd m^{-2}. The efficiency roll-off is only 15% and the EL peak still at 470 nm with a CIE coordinates of (0.15, 0.22). We attribute the high performances of non-doped device to the hybridized local and charge transfer (HLCT) excited state. These results are among the best involving HLCT blue-emissive materials for blue fluorescent OLEDs.

Result and discussion

Synthesis and characterization

The TPAAnPI synthesis route is illustrated in **Scheme 1**. The PPI-Br was synthesized through one-pot reaction of 9,10-phenanthraquinone, 4-aminobenzonitrile, ammonium acetate, and 4-bromobenzaldehyde. The corresponding boron ester, PPIB, was then immediately produced using the PPI-Br crude product. Subsequently, PIAn-Br was formed using a Suzuki coupling reaction between PPIB and 9, 10-dibromoanthracene. Finally, the target product, TPAAnPI, was synthesized through a Suzuki coupling reaction between PIAn-Br and TPAB. Details of the synthesis are provided in the Supporting Information, with the ^{1}H NMR of the intermediate products displayed in Fig. S1-3 †. The purity and chemical structure of TPAAnPI are well characterized by ^{1}H NMR (Fig. S4 †), ^{13}C NMR (Fig. S5 †), mass spectrum (Fig. S6 †), and elemental analysis.

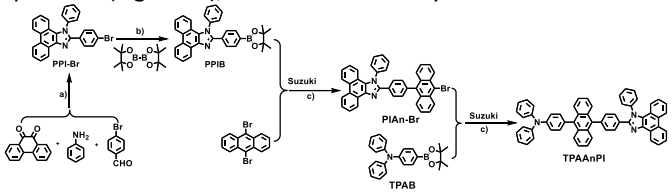

Scheme 1 a) CH_3COONH_4, CH_3COOH, 120°C, N_2 protection, 2 h. b) $Pd(dppf)Cl_2$, KOAc, 1,4-dioxane, 90°C, N_2 protection, overnight. c) K_2CO_3, $Pd(PPh_3)_4$, THF&H_2O, 70°C, 24 h under N_2 protection.

Thermal properties

Thermogravimetric analysis (TGA) and differential scanning calorimetry (DSC) were performed in a nitrogen atmosphere to evaluate the thermal properties of TPAAnPI. As depicted in Fig. S7 †, the decomposition temperature (T_d, corresponding to 5% weight loss) of TPAAnPI is 492°C and the melting point (T_m) is at 366°C, highlighting excellent thermal stability. Simultaneously, a glass-transition temperature (Tg) of 213°C occurs on the DSC curve, indicating excellent morphological stability during heating in industrial production.

Excitation-state properties

Photophysical properties

The ultraviolet (UV-vis) absorption and photoluminescence (PL) spectra of TPAAnPI in THF solution (10^{-5} M) and the evaporated film state are shown in **Fig. 1a**. The TPAAnPI absorption peaks at around 363, 376 and 398 nm are ascribed to the π-π* vibronic fine structure of anthracene moiety,[12] while absorptions in the 300-350 nm range are attributed to the π-π* transition of PI and TPA moieties.[13,14] Notably, the UV absorption spectra hardly changed in terms of both their shape and position as the solvent polarity increasing, implying a rather small dipole moment change at the ground state in different solvents in Fig. S8 †. However, obvious solvatochromic effect of the TPAAnPI is observed in the PL spectra. (**Fig. 1b**) The PL spectra from higher polarity solvents are remarkably broad with red-shifting from 445 nm in n-hexane to 523 nm in acetonitrile as the polarity of the solvents increased. This phenomenon is identical to the high twisting caused by the 9, 10-substitution of anthracene and the separated S3 natural transitional orbit (NTO, **Fig. 2b**). To better understand the solvatochromic effect and further analyse the excited state property of the TPAAnPI, a Lippert-Mataga solvatochromic model is constructed (**Fig. 1c**, Table S1 † and Formula S1 †). A typical two-section linear relation is observed in **Fig. 1c**, where the line with the lesser slope represents the LE-like excited state component with a lower excited state dipole moment (μ_e), while that with the higher slope is for the CT-like excited state component with greater μ_e. This highlights co-existence and hybridization of LE and CT excited state components.[8b] For the TPAAnPI, the calculated lower and larger μ_e is 9.9 D and 25.3 D, respectively. Contrarily, the higher μ_e corresponding to the CT-region is greater than that of the typical CT molecule 4-(N,N-dimethylamino)benzonitrile

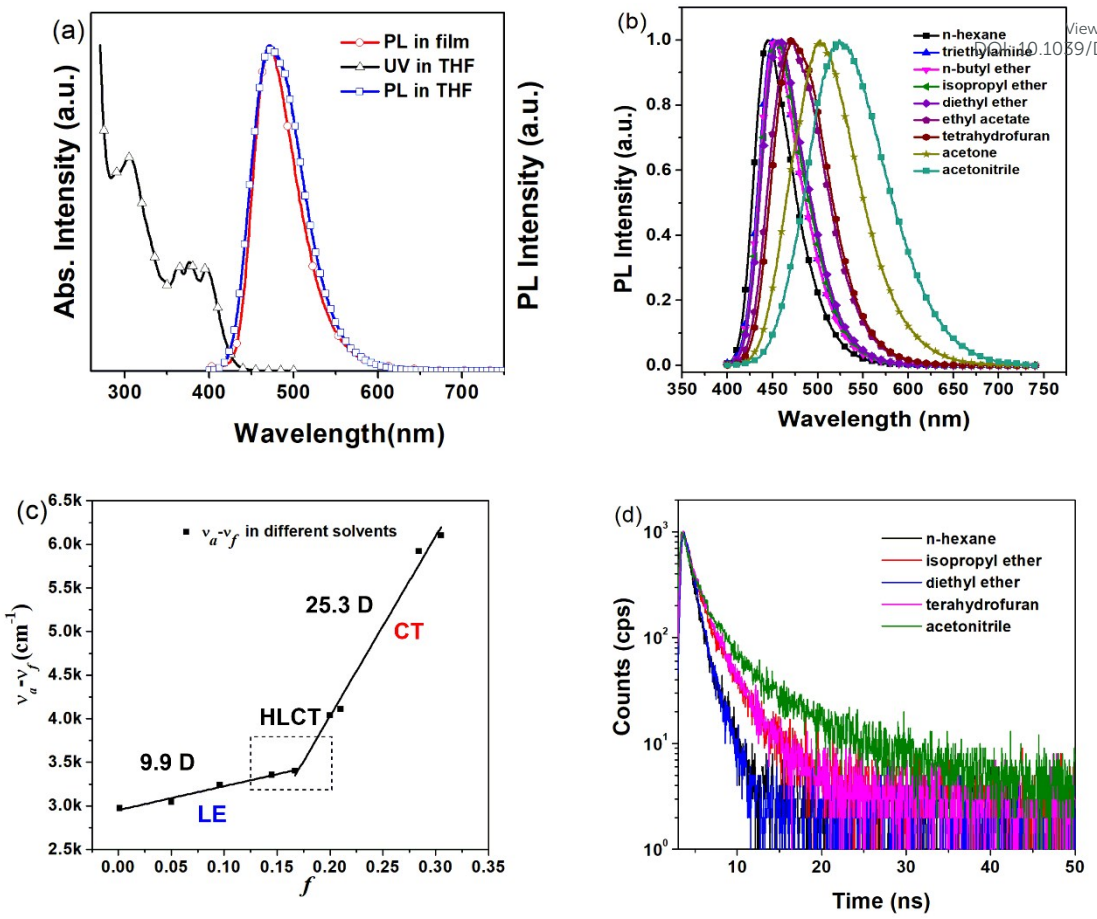

Fig. 1 (a) Normalized UV-vis and PL spectra of TPAAnPI in the THF solution (10^{-5} M) and neat film. (b) Normalized PL spectra of TPAAnPI in nine different solvents with increasing polarity. (c) Linear fitting of Lippert- Mataga model (the solid squares represent the Stocks shifts in different solvents, and the lines are fitted for solvatochromic model), and the ground-state dipole moment (μ_g) was estimated to be 4.0332 D using DFT calculation at the level of M062X/6-31+G(d,p). (d) The transient PL decay spectra of TPAAnPI in different solvents and evaporated film.

(DMABN, 23 D), whereas the μ_e of 9.9 D in the LE-region is a little higher than those for conventional LE molecules such as anthracene and PI, indicating that TPAAnPI is a HLCT material. In low-polarity solvents, the PLQYs remain unchanged (0.54 in n-hexane, 0.54 in isopropyl ether, and 0.58 in diethyl ether), manifesting the LE-dominated emission from the low-lying S_1 state. In a medium-high solvent such as THF, the PLQY reached maximum (0.71), which is attributable to the excellent hybridization of LE and CT excited state. Although in the high-polarity solvents like acetonitrile, the PLQY exhibites a sharp decline, that of the TPAAnPI film still attains 0.42, which is similar to values in the low- and medium- polarity solvents. This provides a satisfactory internal quatum efficiency for the non-doped OLED. As a result, the PLQYs in solvents and film are satisfactory for OLED fabrication. The HLCT character can also be proved according to the single-component, nanosecond scale lifetime of the TPAAnPI solutions (**Fig. 1d**). Additionally, the varied nanosecond fluorescent lifetimes of solutions (1.26 ns in n-hexane, 2.16 ns in isopropyl ether, 1.19 ns in diethyl ether, 2.27 ns in THF and 3.76 ns in acetonitrile) illustrate that high radiative transition rate and a large dipole moment can also exist in the PL process of the TPAAnPI (Table S2 † and Formula S2 †).

Theoretical calculations

Regarding to the HLCT property of TPAAnPI, we investigated its excited state using theoretical methods. First, the molecular configuration and frontier molecular orbital (FMO) of the TPAAnPI were optimized and calculated using the Gaussian 09 B.01 package at the level of M062X/6-31+G(d,p), as shown in **Fig. 2a**. Expectedly, in the 9,10-substituted anthracene derivate, the optimized structure of the TPAAnPI involves a twisted D-π-A molecular configuration with torsional angles of 52.5, 53.7, and 69.0°, respectively. Therefore, the calculated FMO exhibits partial separated characteristics. The highest occupied molecular orbit (HOMO) of the TPAAnPI is mainly localized on the TPA moiety but extends to the adjacent anthrancene moiety. In contrast, the lowest unoccupied molecular orbit (LUMO) is fully distributed on the anthracene moiety, suggesting that the HOMO→LUMO transition involves an intercrossed CT and π-π* transition character, reflecting a typical HLCT character. Furthermore, NTO analysis were performed for the first 10 singlet and 15 triplet excited states based on the S_0 state geometry using the time-dependent DFT (TDDFT) method at the same level as S_0 (**Fig. 2b**, Fig. S9 †). The $S_0 \rightarrow S_1$, and $S_0 \rightarrow S_2$ transitions of the TPAAnPI are the radiative π-π* and non-radiative n-π* transition of anthracene, respectively, which are typical LE transition. The oscillator

View Article Online
DOI: 10.1039/D0SC01341B

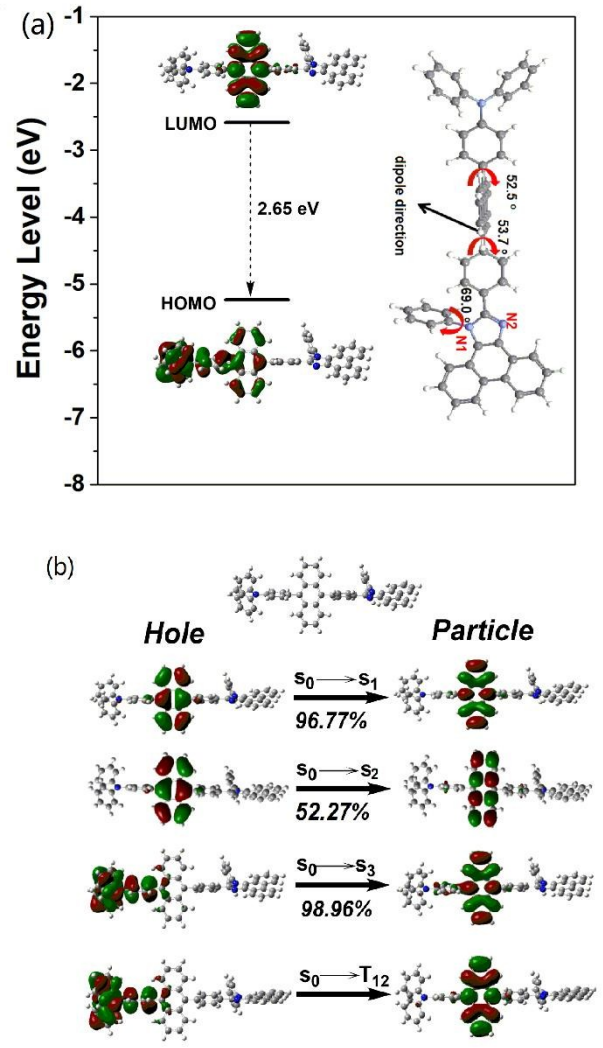

Fig. 2 (a) The frontier molecular orbitals (Highest occupied molecular orbit, HOMO and lowest unoccupied molecular orbit, LUMO) of TPAAnPI and its optimized molecular geometry of ground state (S_0) at the M062X/6-31+G(d,p) level, (b) the NTOs of TPAAnPI for S_0/S_1, S_0/S_2, S_0/S_3 and S_0/T_{12}, S_0: singlet ground state; S_1: the lowest singlet excited state; S_2: the second singlet excited state; S_3: the third singlet excited state; T_{12}: the twelfth triplet excited state. The percentage indicates the possibility of the transition.

strength of the S_1 excited state is 0.5449 which is consistent with the PLQY in the low-polarity solutions such as hexane. We also calculated the excited state dipole moment of the singlet excited state (Table S3 †), obtaining values of 4.16 D and 27.39 D for the S_1 and S_3 states, respectively, which are also in accordance with the experimental results. Therefore, the emissive state of the TPAAnPI belongs to the S_1 excited state, whereas the S_3 excited state serves as the exciton utilization channel. Actually, the S_3 excited state exhibits obvious CT character according to the NTO analysis. The NTO for $S_0 \rightarrow S_3$ transition displays a total CT transition character, with "hole" distributed on the TPA moiety and "particle" distributed on the anthracene with a minor overlap on the adjacent phenyl moiety. The corresponding triplet CT excited state is the T_{12} excited state, and the S_3 -T_{12} energy gap is only 0.0013 eV. Therefore, this could afford efficiently increasing the RISC between S_3 and T_{12} excited states, and eventually improve the EUE.

Electrochemical properties

To understand the electrochemical properties of the TPAAnPI, the HOMO and LUMO energy levels were obtained from the electrochemical cyclic voltammetry measurements (CV) depicted in Fig. S10 † . The onset oxidation and reduction potentials of the TPAAnPI are 0.67 and −2.14 V, with corresponding HOMO and LUMO of -5.24 eV and -2.59 eV, respectively, according to Formula S3 † . (Ferrocene was used as internal standard, $E^+1/2$ vs. Ag/Ag^+ was measured as 0.23 V, $E^-1/2$ vs. Ag/Ag^+ was 0.07 V). The calculated electrical band gap of 2.65 eV is blue-emissive.

Electroluminescence properties

To explore the potential application of the TPAAnPI as an electro-fluorescent material, non-doped blue fluorescent OLED was fabricated. The optimized structures of the devices referred to as Device I and Device II contain the following: Device I: ITO/PEDOT:PSS (40 nm)/TAPC (5 nm)/TCTA (30 nm)/TPAAnPI (20 nm)/TPBi (30 nm)/LiF (1 nm)/Al (100 nm) and Device II: ITO/PEDOT:PSS (40 nm)/TCTA (30 nm)/TPAAnPI (20 nm)/TPBi (30 nm)/LiF (1 nm)/Al (100 nm).The conducting polymer polyethylene dioxythiophene/polystyrene sulfonate (PEDOT:PSS) is served as the hole injecting layer, while di-(4-(N,N-ditolyl-amino)-phenyl) cyclohexan (TAPC) acted as the hole transporting layer. The 4,4',4"-tri(N-carbazolyl)-triphenylamine (TCTA) was used as hole transporting and electron blocking layer, whereas 1,3,5-tri(phenyl-2-benzimidazolyl)benzene (TPBi) represented an electron transporting and hole blocking layer, and LiF the electron injecting layer. The summary properties of Device I and II are presented in **Table 2**.

As shown in **Fig. 3**, Device I exhibited a novel blue emission, with the electroluminescence (EL) emission peak at 470 nm corresponding to the Commission International de L'Eclairage (CIE) coordinates of (0.15,0.22) at 6 V (**Fig. 3 (d)**). Its maximum current efficiency (CE) of 12.51 cd A^{-1} and the maximum power efficiency (PE) of 11.47 lm W^{-1}. It also displayed a maximum luminescence of ≈22489 cd cm^{-2} and maximum external quantum efficiency (EQE) is only of 8.00% at the luminescence of 705 cd m^{-2}. Although the efficiency roll-off ($\eta_{roll\text{-}off}$) is only of 0.75% (according to Formula S4 †) at the luminance of 1000 cd m^{-2}, the EQE remains unsatisfactory in the industrial application. Therefore, the non-dope Device II was fabricated to improve the performances. The optimized non-doped Device II exhibited a maximum CE of 18.09 cd A^{-1} and the maximum PE of 12.35 lm W^{-1}. Its maximum luminescence is ≈29900 cd cm^{-2}, and its maximum EQE of 11.47% corresponding to the high EUE of 91%. More importantly, its EQE remains as high as 9.70% at the luminescence of 1000 cd m^{-2}. Also the $\eta_{roll\text{-}off}$ is only 15% and the EL peak is still at 470 nm with CIE coordinates of (0.15, 0.22) (**Fig. 3 (d)**). Further the EL spectra are stable, with little vibronic features over the entire drive voltage range of 4 V to 8 V (Fig.

View Article Online
DOI: 10.1039/D0SC01341B

ARTICLE

Table 1 Photophysical, electronic energy and thermal properties of TPAAnPI.

Compound	λ_{abs} (s/f) [nm][a)]	λ_{PL} (s/f) [nm][b)]	T_g/T_m [°C][c)]	T_d [°C][d)]	HOMO [eV][e)]	LUMO [eV][e)]	Eg [eV][e)]	η_{PL}(s/f) [%]
TPAAnPI	395/404	470/470	213/366	492	-5.24	-2.59	2.65	71/42

[a)]λ_{abs}(s): maximum absorption wavelength in dilute THF (10^{-5}M); λ_{abs}(f): maximum absorption wavelength in the film; [b)]λ_{PL}(s): emission peak in dilute THF; λ_{PL}(f): emission peak in film; [c)]T_g: glass transition temperature; T_m: melting temperature; [d)]T_d: decomposition temperature; [e)]Measured by cyclic voltammetry measurement; [f)]η_{PL}(s): the fluorescent quantum yield in dilute THF (10^{-5}M); η_{PL}(f): the fluorescent quantum yield in evaporated film.

S11 †). The high EQE and the low $\eta_{roll\text{-}off}$ of Device I and II further highlight a great potential of the TPAAnPI molecule for industrial applications.

Then, the radiative exciton utilization efficiency of Device II was estimated according to the following equation: $\eta_{EL} = \eta_{rec} \cdot \eta_s \cdot \eta_{PL} \cdot \eta_{out}$, where η_{EL} is the EQE of device, η_{rec} denotes the recombination efficiency of the injected holes and electrons, η_{PL} is the PLQY of the emitter, η_s represents the EUE of device, and η_{out} is the light out-coupling efficiency. Assuming an $\eta_{out} \approx 0.3$ for a glass substrate with a refraction index n of 1.5, η_{rec} is 100%, and η_{PL} of the TPAAnPI in solid film state is 42%. Therefore, the calculated η_s is 91%, breaking the limit of 25% limit rule by spin statistics in conventional fluorescent OLEDs,[15] implying almost all triplet excitons are converted to the singlet in the EL process. The recent non-doped blue OLEDs with $CIE_y \approx 0.2$ are listed in Table S4 † .

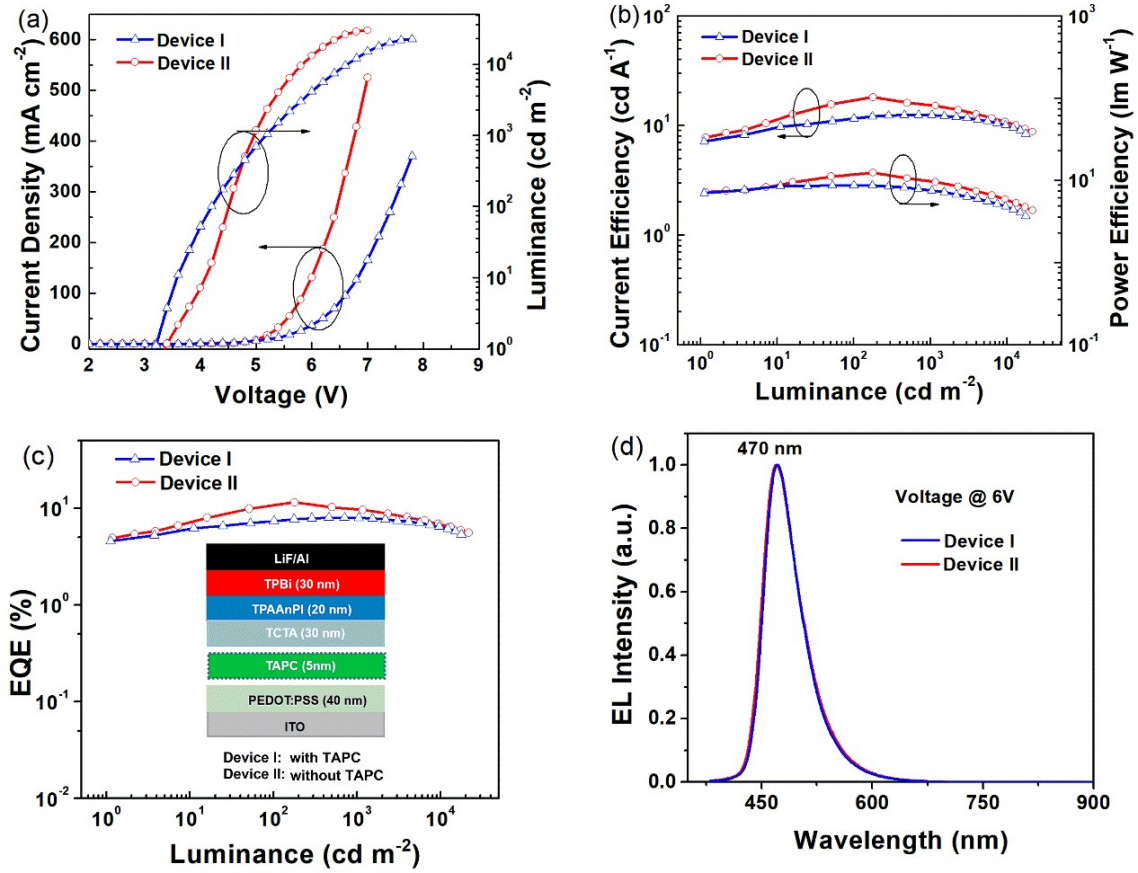

Fig. 3 (a) The current density–voltage–luminance curve of Device I & II. (b) The current efficiency–luminance–power efficiency curves of Device I & II. (c) The external efficiency–luminance curves of Device I & II, the inset shows the device structure diagram. (d) Normalized EL spectra of Device I & II at 6 V.

View Article Online
DOI: 10.1039/D0SC01341B

ARTICLE

Table 2 Electroluminescent properties of device I and II based on TPAAnPI.

Device	$V_{turn-on}$ [V][a]	CE_{max} [cd A^{-1}][b]	PE_{max} [lm W^{-1}][c]	$EQE_{max/1000/10000}$ [%][d]	L_{max} [cd m^{-2}][e]	λ_{EL} [nm][f]	V^{end} [V][g]	CIE [X,Y][h]	$\eta_{roll-off}$ [%][i]
I	3.20	12.51	11.47	8.00/7.94/6.41	22489	470	7.80	0.15,0.22	0.75
II	3.40	18.09	12.35	11.47/9.70/6.80	29900	470	7.00	0.15,0.22	15

[a]Turn on voltage at the luminescence of 1 cd m^{-2}. [b]Maximal current efficiency. [c]Maximal power efficiency. [d]EQE_{max}: Maximal external quantum efficiency; EQE_{1000}: external quantum efficiency at the luminescence of 1000 cd m^{-2}; EQE_{10000}: external quantum efficiency at the luminescence of 10000 cd m^{-2}. [e]Maximum luminescence. [f]Maximal EL peak value. g) End voltage at the luminescence of 1 cd m^{-2}.[h]Observer: 2°; obtained at 6 V; [i]Efficiency roll-off. Device I structure of: ITO/PEDOT:PSS(40 nm)/TAPC(5 nm)/TCTA(30 nm)/TPAAnPI(20 nm)/TPBi (30 nm)/LiF (1 nm)/Al (100 nm); Device II structure: ITO/PEDOT:PSS(40 nm)/TCTA(30 nm)/TPAAnPI(20 nm)/TPBi (30 nm)/LiF (1 nm)/Al (100 nm).

The high η_s is attributed to the novel HLCT mechanism in the EL process. The small energy splitting between S_3 and T_{12} ($\triangle E_{ST} \approx 0$) in **Fig. 4** can create a potential RISC process from T_{12} to S_3. In this way, the triplet excitons are converted to the singlet in the EL process. According to the energy-gap law,[16] the large energy gap between T_2 and T_1 ($\triangle E_{T1T2}$= 1.07 eV) inhibits the internal conversion (IC) process, and the more competitive RISC process between T_{12} and S_3 is prioritized because of the narrower energy gap (Fig. S12 †). Therefore, a large fraction of the electro-generated triplet excitons can turn into singlet excitons through the $T_{12} \rightarrow S_3$ channel. Moreover, the large energy gap ($\triangle E_{ST}$ = 1.35 eV) between S_1 and T_1 prevents the ISC process from the low-lying S_1 to T_1 and excludes the existence of TADF mechanism. More importantly, we measured the transient EL decay curves of Device II at different voltages (Fig. S13 (a) †). The curves are consisted of two components: a rapid EL decay originating from the promote fluorescence of S_1 and a delayed one. The delayed one is due to the collision recombination of previously injected holes and electrons which stayed in the emitter layer after voltage off.

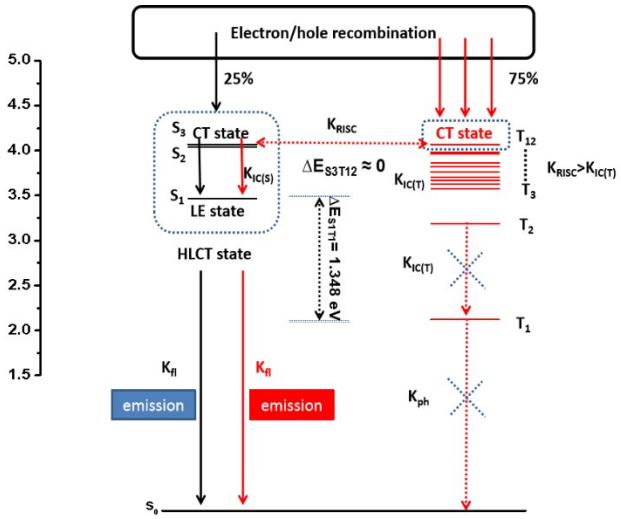

Fig. 4 Model for exciton relaxation in the EL process. RISC: reverse intersystem crossing; IC(T): internal conversion between the triplet states; IC(S): internal conversion between the singlet states; fl: fluorescence; ph: phosphorescence.

The amplified delayed component was obtained by taking the logarithm of EL intensity as Y and the logarithm of time as X, the slope of the obtained curve is -0.28 in the initial time and -1.29 at the long lived EL transient (in Fig. S13 (b) †). According to Monkman *et al.*,[17] if TTA mechanism is predominant in Device II, the delayed EL intensity should be proportional to t^{-2} at the long lived EL transient and the obtained slope should be -2 instead of -1.29. We further compared the transient EL decay curves at different driving voltages of Device II with a typical TTA device based on MADN (Fig. S13 (c) †). The EL intensity of Device II decays much faster than MADN-based device. As the driving voltage increased from 6 V to 8 V, the ratio of delayed component of MADN-based device decreased due to the enhanced triplet excitons quenching process. However, the delayed component of Device II exhibited a much shorter decay time and showed no obvious dependence on the driving voltage. The above results suggested that the contribution of the TTA is insignificant in the EL process. Therefore, the HLCT mechanism is likely responsible for the radiative exciton ratio above 25% in the non-doped OLED based on the TPAAnPI molecule.

Conclusions

In summary, a twisting novel blue D-π-A molecule, TPAAnPI, involving the HLCT excited state was designed and synthesized. The HLCT character was demonstrated by photophysical experiments and DFT analysis. A fabricated optimized non-doped Device II based on TPAAnPI exhibited a maximum EQE of 11.47% and showed a novel blue emission at 470 nm with CIE coordinates of (0.15, 0.22). More importantly, the EQE remained as high as 9.70% at the luminescence of 1000 cd m^{-2} with $\eta_{roll-off}$ of only 15%. The maximum EQE was only 8.00% for Device I, with almost negligible $\eta_{roll-off}$ of 0.75% at a luminance of 1000 cd m^{-2}. These results are among the best for non-doped blue fluorescent OLEDs of HLCT blue-emissive materials. Our study therefore, proposed a molecular design method for a blue-emissive HLCT material characterized by a high radiative exciton ratio, high EQE, and low $\eta_{roll-off}$. These results are

beneficial for further exploring molecular design and device optimization that can maximize triplet to singlet exciton up-conversion involving the HLCT mechanism. We believe that our results are valuable for improved practical applications in display and lightings.

Experimental section

Materials: All raw materials were commercially purchased from Aldrich Chemical Co. or Energy Chemical Co., China and used without further purification unless otherwise noted. Tetrahydrofuran (THF) was dried and purified by fractional distillation over sodium/benzophenone before use.

Measurements: The ^{1}H NMR and ^{13}C NMR spectra were recorded on a Bruker AC500 spectrometer at 500 and 125 MHz, respectively, using deuterated chloroform ($CDCl_3$) or dimethyl sulphoxide (DMSO) as solvents. The chemical shift for each signal was reported in ppm units with tetramethylsilane (TMS) as a standard internal reference. The MALDI-TOF-MS mass spectra were recorded using an AXIMA-CFRTM instrument. The compounds were characterized by a Flash EA 1112, CHN elemental analysis instrument.

Device fabrication and characterization: The two typical device configurations fabricated by vacuum deposition were ITO/PEDOT: PSS (40 nm)/TCTA (30 nm)/TPAAnPI (20 nm)/TPBi (30 nm)/LiF (1 nm)/Al (100 nm) and ITO/PEDOT: PSS (40 nm)/TAPC (5 nm)/TCTA (30 nm)/TPAAnPI (20 nm)/TPBi (30 nm)/LiF (1 nm)/Al (100 nm). ITO-coated glass with a sheet resistance of 10 Ω square^{-1} and it was used as the substrate. The pre-treatment of ITO glass included a routine chemical cleaning using detergent and alcohol in sequence, dried in an oven at 120 °C. After then oxygen plasma cleaning it for 4 min and finally transferred it to a vacuum deposition system with a base pressure greater than 5×10^{-6} mbar for organic and metal deposition. The PEDOT (polyethylene dioxythiophene) and PSS (polystyrene sulfonate) mixture layer was deposited onto the ITO-coated substrate as the hole-injection layer. The cathode LiF was deposited by thermo-evaporation and followed by a thick Al capping layer. The current–voltage–luminance characteristics were measured by using a Keithley source measurement unit (Keithley 2400 and Keithley 2000) with a calibrated silicon photodiode. The electroluminescent (EL) spectra and Commission Internationale de l'Eclairage (CIE) coordinates of these devices were measured by a PR650 spectroscan spectrometer. EQEs were calculated from the luminance, current density, and EL spectrum, assuming a Lambertian distribution. (Formula S5 †) All the results were measured in the forward-viewing direction without using any light outcoupling technique.

Synthesis of TPAAnPI: A mixture of PIAn-Br (0.95g, 1.52 mmol), N,N-diphenyl-4-(4,4,5,5-tetramethyl-1,3,2-dioxaborolan-2-yl)aniline (0.53 g, 1.83 mmol), K_2CO_3 (0.31 g, 2.24 mmol), tetrahydrofuran (THF, 50 ml) and deionized water (H_2O, 10 ml), with $Pd(PPh_3)_4$ (0.05 g, 0.043 mmol) acting as catalyst was refluxed at 70 °C for 24 h under nitrogen. After the mixture was cooled down, 50 ml H_2O was added to the resulting solution and the mixture was extracted with dichloromethane for several times. The organic phase was dried over $MgSO_4$. After filtration and solvent evaporation, the given residue was purified through silica gel column chromatography using dichloromethane/petroleum ether (3:1; v/v) as eluent to give the product as light yellow solid (0.90 g, 75%). ^{1}H NMR (500 MHz, Chloroform-*d*) δ= 8.97 (d, J = 7.9 Hz, 1H), 8.81 (d, J = 8.4 Hz, 1H), 8.75 (d, J = 8.3 Hz, 1H), 7.85 (dd, J = 8.3, 5.9 Hz, 4H), 7.79 (t, J = 7.5 Hz, 1H), 7.73 – 7.64 (m, 8H), 7.54 (t, J = 7.7 Hz, 1H), 7.46 – 7.30 (m, 15H), 7.27 (d, J = 9.0 Hz, 6H), 7.09 (t, J = 7.2 Hz, 2H). ^{13}C NMR (126 MHz, $CDCl_3$) δ= 150.75, 147.78, 147.17, 139.81, 138.85, 137.56, 137.25, 136.08, 132.48, 132.08, 131.33, 130.23, 130.03, 129.94, 129.77, 129.38, 129.33, 129.22, 128.31, 127.32, 127.26, 127.10, 126.79, 126.31, 125.66, 125.11, 124.97, 124.69, 124.14, 123.08, 122.81, 120.91, 77.26, 77.01, 76.76, 53.41. MALDI-TOF MS (mass *m/z*): 789.29 [M^+]. Anal. calcd for $C_{59}H_{39}N_3$: C, 89.70; H, 4.98; N, 5.32, Found: C, 89.43; H, 5.00; N, 5.57.

Conflicts of interest

There are no conflicts to declare.

Acknowledgements

We are grateful for financial support from the National Science Foundation of China (No. 51873095, 51673105 and 51803071), the Key Project of Higher Educational Science and Technology Program of Shandong Province of China (No. J18KZ001), and the Natural Science Foundation of Qingdao City of China (No. 16-5-1-89-jch). We thank Open Project of the State Key Laboratory of Supramolecular Structure and Materials of Jilin University (SKLSSM-202032). We appreciate that the State Key Laboratory of Luminescent Materials and Devices of South China University of Technology provides convenience for fabricating OLED devices.

References

1 (a) C. W. Tang and S. A. VanSlyke, *Appl. Phys. Lett*., 1987, **51**, 913-915; (b) M. A. Baldo, D. F. O'Brien, Y. You, A. Shoustikov, S. Sibley, M. E. Thompson and S. R. Forrest, *Nature,* 1998, **395**, 151−154; (c) A. C. Grimsdale, K. L. Chan, R. E. Martin, P. G. Jokisz and A. B. Holmes, *Chem. Rev*., 2009, **109**, 897−1091.

2 (a) Y. Cao, I. D. Parker, G. Yu, C. Zhang and A. J. Heeger, *Nature,* 1999, **397**, 414−417; (b) S. Krotkus, D. Kasemann, S. Lenk, K. Leo and S. Reineke, *Light Sci. Appl.,* 2016, **5**, e16121; (c) J. Lee, M. Slootsky, K. Lee, Y. Zhang and S. R. Forrest, *Light Sci. Appl.,* 2014, **3**, e181; (d) W. H. Lee, Z. Zhao, Y. J. Cai, Z. Xu, Y. Yu, Y. Xiong, R. T. K. Kwok, Y. Chen, N. L. C. Leung, D. G. Ma, J. W. Y. Lam, A. J. Qin and B. Z. Tang, *Chem. Sci.,* 2018, **9**, 6118−6125; (e) C. L. Li, J. B. Wei, X. X. Song, K. Q. Ye, H. Y. Zhang, J. Y. Zhang and Y. Wang, *J. Mater. Chem. C*, 2016, **4**, 7013−7019; (f) C. L.

Li, S. P. Wang, W. P. Chen, J. B. Wei, G. C. Yang, K. Q. Ye, Y. Liu and Y. Wang, *Chem. Commun*., 2015, **51**, 10632−10635.

3 (a) K. Udagawa, H. Sasabe, C. Cai and J. Kido, *Adv. Mater.,* 2014, **26**, 5062−5066; (b) J.-H. Lee, S.-H. Cheng, S.-J. Yoo, H. Shin, J.-H. Chang, C.-I. Wu, K.-T. Wong and J.-J. Kim, *Adv. Funct. Mater.,* 2015, **25**, 361−366; (c) T. Suzuki, Y. Nonaka, T. Watabe, H. Nakashima, S. Seo, S. Shitagaki and S. Yamazaki, *Jpn. J. Appl. Phys.,* 2014, **53**, 052102; (d) T. B. Njuyan, H. Nakanotani, T. Hatakeyama and C. Adachi, *Adv. Mater.,* 2020, 1906614; (e) L. Yu, Z. B. Wu, G. H. Xie, W. X. Zeng, D. G. Ma and C. L. Yang, *Chem. Sci.,* 2018, **9**, 1385-1391; (f) Z. Q. Li, C. L. Li, Y. C. Xu, N. Xie, X. C. Jiao and Y. Wang, *J. Phys. Chem. Lett*., 2019, **10**, 842−847.

4 (a) Y. L. Zhang, Q. Ran, Q. Wang, Y. Liu, C. Hanisch, S. Reineke, J. Fan and L. S. Liao, *Adv. Mater.,* 2019, **31**, 1902368; (b) Q. Wang and D. G. Ma, *Chem. Soc. Rev*., 2010, **39**, 2387−2398; (c) H.-H. Chou, Y.-H. Chen, H.-P. Hsu, W.-H. Chang, Y.-H. Chen and C.-H. Cheng, *Adv. Mater*., 2012, **24**, 5867−5871. (d) N. Sharma, E. Spuling, C. M. Mattern, W. B. Li, O. Fuhr, Y. Tsuchiya, C. Adachi, S. Brase, I. D. W. Samuel and E. Z.-Colman, *Chem. Sci.,* 2019, **10**, 6689−6696; (e) C. L. Li, Z. Q. Li, X. J. Yan, Y. W. Zhang, Z. L. Zhang and Y. Wang, *J. Mater. Chem. C*, 2017, **5**, 1973−1980; (f) C. L. Li, J. B. Wei, J. X. Han, Z. Q. Li, X. X. Song, Z. L. Zhang, J. J. Zhang and Y. Wang, *J. Mater. Chem. C*, 2016, **4**, 10120−10129.

5 (a) H. Sasabe, J. Takamatsu, T. Motoyama, S. Watanabe, G. Wagenblast, N. Lange, O. Molt, E. Fuchs, C. Lennartz and J. Kido, *Adv. Mater.,* 2010, **22**, 5003−5007; (b) T. Fleetham, G. J. Li, L. L. Wen and J. Li, *Adv. Mater.,* 2014, **26**, 7116−7121; (c) C. L. Li, Z. Q. Li, J. X. Liang, H. Luo, Y. Liu, J. B. Wei and Y. Wang , *J. Mater. Chem. C*, 2018, **6**, 12888−12895; (d) Z. Q. Li, Z. Cheng, J. Y. Lin, N. Xie, C. L. Li, G. C. Yang and Y. Wang, *J. Mater. Chem. C*, 2019, **7**, 13486−13492.

6 (a) S. Kappaun, C. Slugovc, J. W. List, *Int. J. Mol. Sci.,* 2008, **9**, 1527−1547; (b) G. Cheng, S. C. F. Kui, W.-H. Ang, M.-Y. Ko, P.-K. Chow, C.-L. Kwong, C.-C. Kwok, C. S. Ma, X. G. Guan, K.-H. Low, S.-J. Su and C.-M. Che, *Chem. Sci.,* 2014, **5**, 4819−4830; (c) Y. Kawamura, K. Goushi, J. Brooks, J. J. Brown, H. Sasabe and C. Adachi, *Appl. Phys. Lett.,* 2005, **86**, 071104; (d) V. Sivasubramaniam, F. Brodkorb, S. Hanning, H. P. Loebl, V. van Elsbergen, H. Boerner, U. Scherf and M. Kreyenschmidt, *J. Fluorine Chem.,* 2009, **130**, 640−649; (e) K. Klimes, Z. Q. Zhu and J. Li, *Adv. Funct. Mater.,* 2019, **29**, 1903068.

7 (a) Q. S. Zhang, B. Li, S. P. Huang, H. Nomura, H. Tanaka and C. Adachi, *Nat. Photonics,* 2014, **8**, 326−332; (b) H. Uoyama, K. Goushi, K. Shizu, H. Nomura and C. Adachi, *Nature,* 2012, **492**, 234−238; (c) X. K. Liu, Z. Chen, J. Qing, W. J. Zhang, B. Wu, H. L. Tam, F. R. Zhu, X. H. Zhang and C. S. Lee, *Adv. Mater*., 2015, **27**, 7079−7085; (d) D. X. Ding, Z. C. Wang, C. Y. Li, J. Zhang, C. B. Duan, Y. Wei and H. Xu, *Adv. Mater.,* **2020**, 1906950. (e) I. S. Park, H. Komiyama and T. yasuda, *Chem. Sci.,* 2017, **8**, 953−960.

8 (a) W. J. Li, D. D. Liu, F. Z. Shen, D. G. Ma, Z. M. Wang, T. Feng, Y. X. Xu, B. Yang and Y. G. Ma, *Adv. Funct. Mater.,* 2012, **22**, 2797−2803; (b) S. T. Zhang, W. J. Li, L. Yao, Y. Y. Pan, F. Z. Shen, R. Xiao, B. Yang and Y. G. Ma, *Chem. Commun.,* 2013, **49**, 11302−11304; (c) S. T. Zhang, L. Yao, Q. M. Peng, W. J. Li, Y. Y. Pan, R. Xiao, Y. Gao, C. Gu, Z. M. Wang, P. Lu, F. Li, S. J. Su, B. Yang and Y. G. Ma, *Adv. Funct. Mater.,* 2015, **25**, 1755−1762; (d) C. J. Zhou, D. L. Cong, Y. Gao, H. C. Liu, J. Y. Li, S. T. Zhang, Q. Su, Q. L. Wu and B. Yang, *J. Phys. Chem. C,* 2018, **122**, 18376−18382; (e) S. F. Xue, X. Qiu, S. A. Ying, Y. S. Lu, Y. Y. Pan, Q. K. Sun, C. Gu, and W. J. Yang, *Adv. Optical Mater*., 2017, **5**, 1700747; (f) J. J. Shi, Q. Ding, L. Xu, X. H. Lv, Z. W. Liu, Q. K. Sun, Y. Y. Pan, S. F. Xue and W. J. Yang, *J. Mater. Chem. C*, 2018, **6**, 11063−11070.

9 (a) D. R. Lee, M. Kim, S. K. Jeon, S. H. Hwang, C. W. Lee and J. Y. Lee, *Adv. Mater.,* 2015, **27**, 5861-5867; (b) M. Kim, S. K. Jeon, S.-H. Hwang, S.-S. Lee, E. Yu and J. Y. Lee, *J. Phys. Chem. C,* 2016, **120**, 2485−2493.

View Article Online DOI: 10.1039/D0SC01341B

10 (a) D. D. Zhang, M. H. Cai, Y. G. Zhang, D. Q. Zhang and L. Duan, *ACS Appl. Mater. Interfaces,* 2015, **7**, 28693−28700; (b) D. D. Zhang, L. Duan, C. Li, Y. L. Li, H. Y. Li, D. Q. Zhang and Y. Qiu, *Adv. Mater.,* 2014, **26**, 5050-5055; (c) H. Nakanotani, T. Higuchi, T. Furukawa, K. Masui, K. Morimoto, M. Numata, H. Tanaka, Y. Sagara, T. Yasuda and C. Adachi, *Nat. Commun.,* 2014, **5**, 4016.

11 (a) W. J. Li, Y. Y. Pan, R. Xiao, Q. Peng, S. T. Zhang, D. G. Ma, F. Li, F. Z. Shen, Y. Wang, B. Yang and Y. G. Ma, *Adv. Funct. Mater.,* 2014, **24**, 1609−1614; (b) H. C. Liu, Q. Bai, W. J. Li, Y. C. Guo, L. Yao, Y. Gao, J. Y. Li, P. Lu, B. Yang and Y. G. Ma, *RSC Adv.,* 2016, **6**, 70085−70090; (c) X. Y. Tang, Q. Bai, Q. M. Peng, Y. Gao, J. Y. Li, Y. L. Liu, L. Yao, P. Lu, B. Yang and Y. G. Ma, *Chem. Mater.,* 2015, **27**, 7050−7057. (d) H. C. Liu, Q. Bai, L. Yao, H. Y. Zhang, W. J. Li, Y, Gao, J. Y. Li, P. Lu, H. Y. Wang, B. Yang and Y. G. Ma, *Chem. Sci.,* 2015, **6**, 3797−3804.

12 R. N. Jones, *Chem. Rev.,* 1947, **41**, 353−371.

13 Z. Gao, Y. L. Liu, Z. M. Wang, F. Z. Shen, H. Liu, G. N. Sun, L. Yao, Y. Lv, P. Lu and Y. G. Ma, *Chem. – Eur. J.,* 2013, **19**, 2602−2605.

14 S. Tang, W. J. Li, F. Z. Shen, D. D. Liu, B. Yang and Y. G. Ma, *J. Mater. Chem.,* 2012, **22**, 4401−4408.

15 S. J. Su, E. Gonmori, H. Sarabe and J. Kido, *Adv. Mater.,* 2008, **20**, 4189−4194.

16 N. J. Turro, *Modern Molecular Photochemistry*, University Science Books, Sausalito, CA, USA, 1991.

17 C. Rothe and A. P. Monkman, *Phys. Rev. B,* 2003, **68**, 075208.

View Article Online
DOI: 10.1039/D0SC01341B

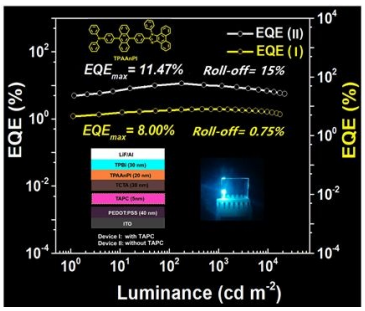

A new pure fluorescent blue HLCT-emitter was designed and synthesized. Highly efficient non-doped blue OLEDs with low efficiency roll-off were achieved.